Proceedings of the 42nd IEEE
Conference on Decision and Control
Maui, Hawaii USA, December 2003

Robust Model-based Fault Detection For Roll Rate Sensor

H. E. Tseng Li Xu

Ford Motor Company
Dearborn, MI 48124
Email: htseng@ford.com, lxu9@ford.com

Abstract

Due to the wide variation of vehicle dynamics under a vast operating range, such as dynamically changing road super-elevations and road grades, the detection of a roll rate signal fault using analytical redundancy is particularly challenging. These challenges, as well as the robustness and performance of the proposed scheme are discussed. The robust performance of the proposed scheme, over model uncertainties and road disturbances, is illustrated analytically and validated through simulations and experiments. The analytical illustrations include three elements: a robust estimation of the vehicle roll angle, a dynamic compensation of both electrical and kinematics-induced bias in the roll rate signal, and a directionally sensitive design of a robust observer which decouples the model uncertainties and disturbances from the fault.

1 Introduction

Recently, Ford has developed a brake actuation systems to enhance on-road vehicle roll stability [1]. The Ford Roll Stability Control (RSC) system utilizes a sensor set to detect the dynamic condition of the vehicle and a controller to distribute brake pressure for reducing lateral tire forces that contribute to the detected roll instability. The sensor set includes four wheel speed sensors, a steering wheel sensor, a lateral acceleration sensor, a yaw rate sensor, and a roll rate sensor. The roll rate sensor is the only additional sensor on top of a yaw stability enhancing Electronic Stability Control (ESC) equipped vehicle [2], and can be used to provide RSC with critical feedback information. Failures of the roll rate sensor in an RSC equipped vehicle, therefore, must be rapidly diagnosed to ensure proper system activations.

In this paper, a fault detection scheme using analytical redundancy is considered. Fault detections using analytical redundancy can be categorized into knowledge based approaches and model based approaches [3]. Among the model based detection processes in which we are interested, a robust observer design using eigenstructure assignment is believed to offer a better robustness over voting schemes, Kalman filter based approaches, etc. The impact of an inaccurate model on Kalman filter based approaches was examined by [4] and the robustness advantage of robust observer design was suggested in [5]. For roll rate sensor fault detection, this is particularly appealing due to large unknown roll disturbances and roll model uncertainties encountered in a vehicle.

While fault detection methodologies using eigenstructure assignment have previously been developed for other systems [5, 6, 7], the roll rate fault detection problem at hand poses a few unique challenges. The vehicle roll angle is not directly measurable and the roll rate signal to be examined may contain time-varying and significant bias that cannot be considered as a fault. Therefore, in addition to finding a proper vehicle roll model and constructing a robust observer using this methodology, the vehicle roll angle has to be estimated and the time-varying, maneuver dependent bias has to be compensated. Furthermore, due to the wide variation of vehicle dynamics under a vast operating range, such as various and dynamically changing road super-elevations and road grades, the magnitude of disturbances existing in the roll rate signal and roll angle estimate is significant and the detection of a roll rate signal fault using analytical redundancy is particularly challenging.

2 Robust Fault Observer Using Eigenstructure Assignment

Considering the significant variations a vehicle may experience in practice, there is a need to develop robust fault detection algorithms in which the sensor fault is decoupled from model uncertainties and disturbances, and the residual is sensitive only to sensor fault. One way to achieve this is to use the eigenstructure assignment approach [5, 6, 7].

Consider a class of linear systems, in which the system uncertainty can be summarized as an additive unknown disturbance term in the dynamic equation described as follows:

$$\begin{aligned} \dot{x} &= Ax + Bu + E\vec{d}, \\ y &= Cx + Du + f_s, \end{aligned} \tag{1}$$

where x is the state vector, u is the input vector, y is the output vector, and f_s is the sensor fault. $\vec{d}$ denotes disturbances acting upon the system, and its distribution matrix E is assumed to be known. A, B, C and D are system model matrices with proper dimensions. Let the state and output estimations be $\hat{x}$ and $\hat{y}$. A state observer for system (1) is given by

$$\begin{aligned} \dot{\hat{x}} &= A\hat{x} + Bu + K(y - \hat{y}), \\ \hat{y} &= C\hat{x} + Du, \end{aligned} \tag{2}$$

where K is the observer gain. Define the state estimation error as $e = x - \hat{x}$. The error dynamics becomes

$$\dot{e} = \dot{x} - \dot{\hat{x}} = (A - KC)e + E\tilde{d} - Kf_s. \quad (3)$$

Now the residual generator can be formed by pre-multiplying the output estimation error with a weighting matrix W as

$$r(t) = W(y - \hat{y}) = W(Cx + f_s - C\hat{x}) = W(Ce + f_s). \quad (4)$$

The Laplace transformed residual response to faults and disturbances is thus

$$r(s) = WC(sI - A_c)^{-1}[E\tilde{d} - Kf_s] + Wf_s, \quad (5)$$

where s is the Laplace operator and $A_c = A - KC$ is the close loop matrix. The disturbance decoupling condition can be easily seen from above as

$$G_{rd}(s) = WC(sI - A_c)^{-1}E = 0. \quad (6)$$

The problem is now reduced to find K and W such that (6) is satisfied and A_c is stable. The assignment of the observer's eigenvectors and eigenvalues is a direct way to solve this problem [6].

Theorem 1 *If $WCE = 0$ and all rows of the matrix WC are left eigenvectors of A_c corresponding to p eigenvalues of A_c, then equation (6) is satisfied [6]. Note p is the dimension of the residual.*

3 Robust Observer for Roll Rate Fault Detection

3.1 Plant Model and Robust Observer Design

In order to utilize the observer design technique discussed above, the selection of the observed plant model is a significant design step. While many models describing vehicle roll dynamics are available in the literature [8, 9], they are not designed for fault detection purpose. On the one hand, these models are all based on multibody dynamics which is highly nonlinear and cannot be utilized to formulate the robust fault observer. On the other hand, they are not sophisticated enough to handle road super-elevations well. Therefore it is essential to find a model that meets the necessary conditions of Theorem 1. Furthermore, it would be advantageous if the model's parametric uncertainties lie in the same subspace (of the state space) as the external disturbances.

To facilitate the robust observer design, a simple linear time-varying roll model incorporating both kinematics and dynamics relationships is chosen as follows:

$$\frac{d}{dt}\begin{bmatrix} \phi \\ \dot{\phi} \end{bmatrix} = \begin{bmatrix} 0 & 1 \\ -k + \Delta k & -c + \Delta c \end{bmatrix}\begin{bmatrix} \phi \\ \dot{\phi} \end{bmatrix} + \begin{bmatrix} 0 \\ 1 \end{bmatrix} d, \quad (7)$$

where ϕ and $\dot{\phi}$ represent vehicle roll angle and roll rate respectively, k and c are the nominal values of effective roll stiffness and damping coefficient, which include suspension geometry and other kinematics effects and have been normalized for vehicle roll inertia, Δk and Δc represent parametric uncertainties and/or nonlinearities which may further be time-varying, and d represents an external disturbance (i.e., roll moment) applied to the vehicle. The output measurements y is selected as follows:

$$y = \begin{bmatrix} \phi \\ \dot{\phi} \end{bmatrix} + \begin{bmatrix} f_\phi \\ f_{d\phi/dt} \end{bmatrix}, \quad (8)$$

where f_ϕ and $f_{d\phi/dt}$ denote roll angle and roll rate sensor faults or measurement errors, respectively.

While the model representation is in a simple format, its parameters can be nonlinear and time-varying in order to capture the roll dynamics under various conditions. For example, constant valued effective roll stiffness and damping coefficients may be sufficient to describe small suspension roll motions while these parameters may have to be nonlinear in order to reflect vehicle roll during large suspension motions. Moreover, the effective roll stiffness and damping (for Euler roll angle) drops significantly when a vehicle stays on a banked road or when a vehicle lifts off the ground.

Noting that both parametric uncertainties and disturbance appear in the second equation of (7), the roll model can be rewritten as

$$\begin{aligned} \dot{x} &= Ax + E\tilde{d}, \\ y &= Cx + f_s, \end{aligned} \quad (9)$$

where

$$x = \begin{bmatrix} \phi \\ \dot{\phi} \end{bmatrix}, A = \begin{bmatrix} 0 & 1 \\ -k & -c \end{bmatrix}, E = \begin{bmatrix} 0 \\ 1 \end{bmatrix}, f_s = \begin{bmatrix} f_\phi \\ f_{d\phi/dt} \end{bmatrix}, \quad (10)$$

$C = I_2$ and $\tilde{d} = d + \Delta k\phi + \Delta c\dot{\phi}$.

Note that (9) belongs to the class of systems described by (1) (with $B = 0$ and $D = 0$). Thus the robust observer design presented in Section 2 can be applied directly to generate a scalar residual which is insensitive to both parametric uncertainties and disturbances:

$$\begin{aligned} \dot{\hat{x}} &= A\hat{x} + K(y - \hat{y}), \\ \hat{y} &= C\hat{x}, \\ r &= W(y - \hat{y}), \end{aligned} \quad (11)$$

where

$$W = [1 \;\; 0], \;\; K = \begin{bmatrix} \lambda_1 & 1 \\ -k & -c + \lambda_2 \end{bmatrix}. \quad (12)$$

It is seen that the observer poles (or eigenvalues of A_c) can be chosen arbitrarily as $-\lambda_1$ and $-\lambda_2$, and the necessary conditions of Theorem 1 are satisfied.

However, there remain two challenges in obtaining the output defined in (8). One is to obtain a roll angle measurement relative to the horizon, or Euler roll angle of the vehicle ϕ. The other one is to obtain the Euler roll rate $\dot{\phi}$ from the roll rate sensor signal.

3.2 Roll Angle "Measurement" - Euler Roll Angle Estimation

The vehicle Euler roll angle is measured in an inertial frame. It includes both a road bank angle (or super-elevation) and a suspension roll angle assuming the wheel plane is parallel to the super-elevation of the road. Both the road bank angle and

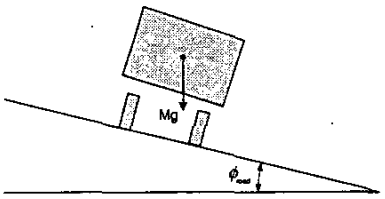

Figure 1: Road Bank

the suspension roll angle are first estimated. The two angles are then merged using an arbitration scheme that further processes them in order to assure the two processed components are mutually exclusive before the final summation.

3.2.1 Road Bank Roll Angle Estimation: A reasonable search within the literature reveals that few studies/documentations discuss the estimation of the super elevation of a road. Among them, Fukada [10] first estimated road bank by comparing an estimated lateral velocity derivative with the difference between lateral acceleration and the product of yaw rate and vehicle speed. The lateral velocity derivative estimate he used, in turn, depends on a low-pass filter version of estimated road bank. Nishio *et al* [11] used a low-pass filter version of the difference between lateral acceleration and the product of yaw rate and vehicle speed as a road bank estimate. Tseng [12] first provided a road bank estimate independent of a side slip angle estimation. In this paper, the calculation process of the road bank estimate proposed in [12] is simplified, and the fidelity of this estimate is further improved by decomposing the estimate into multiple frequency layers and applying a different weighting factor at each layer.

Considering the road bank disturbance (Fig.1), the measurement of the lateral accelerometer is given by

$$a_y = \dot{v} + u \cdot \omega_z + g \cdot \sin\phi_{road}, \tag{13}$$

where a_y is lateral acceleration, u is longitudinal velocity, ω_z is yaw rate, v is lateral velocity, ϕ_{road} represents road bank angle, and g is the gravitational constant. It follows that

$$\sin\phi_{road} = (a_y - \dot{v} - u \cdot \omega_z)/g. \tag{14}$$

However, since $\dot{v}$ is not available, (14) cannot be implemented. To overcome this technical difficulty, a dynamic road bank estimate was suggested by Tseng [12] as,

$$\sin\hat{\phi}_{dyn} = \sin\hat{\phi}_v \cdot \max\left[0, 1 - |DFC| - |\mathrm{d}\sin\hat{\phi}_v/\mathrm{d}t|\right], \tag{15}$$

where

$$\sin\hat{\phi}_v = (a_y - u \cdot \omega_z)/g, \tag{16}$$

and

$$DFC = H_{\phi\to a}(\sin\hat{\phi}_a - \sin\hat{\phi}_v) + u \cdot H_{\phi\to\omega}(\sin\hat{\phi}_\omega - \sin\hat{\phi}_v), \tag{17}$$

in which

$$\begin{aligned} \sin\hat{\phi}_\omega &= H^{-1}_{\phi\to\omega}(\omega_z - H_{\delta\to\omega}\delta), \\ \sin\hat{\phi}_a &= H^{-1}_{\phi\to a}(a_y - H_{\delta\to a}\delta), \end{aligned} \tag{18}$$

where δ is front tire steer angle and the transfer functions $H_{\phi\to\omega}$, $H_{\delta\to r}$, $H_{\phi\to a}$ and $H_{\delta\to a}$ represent the input/output relations between steering input and sensor measurements as well as those between road bank disturbances and sensor measurements [12]. It can be shown that the dynamic factor, DFC, can be further simplified if we substitute the transfer functions above with their DC gains, and a formula that reduces real-time computational load is given by,

$$DFC = \frac{2u^2}{g(L + k_u u^2)} \cdot \left[k_u \cdot a_y + \frac{\omega_z}{u} \cdot L - \delta\right], \tag{19}$$

where L is wheelbase and k_u is understeer coefficient. Note that the expression in the bracket is zero during steady-state cornering of a vehicle if the bicycle model and its nominal understeer coefficient is accurate [13].

An empirical study shows that the fidelity of the estimated vehicle roll angle can further be improved by modulating differently in different frequency layers (Fig.2). The estimated

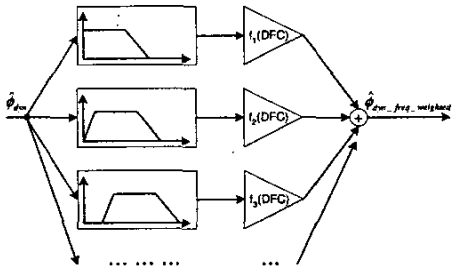

Figure 2: Frequency Weighted Road Bank Angle

value of road bank angle is denoted as $\hat{\phi}_{dyn\_freq\_weighted}$. The need of a frequency dependent multiplication scheme to improve the estimate can be interpreted as the fidelity of the bicycle model and its corresponding understeer coefficient may be frequency dependent.

3.2.2 Suspension Roll Angle Estimation: Using a single mass-spring suspension (or sprung mass) roll model [9], a dynamic relation between the suspension roll rate and roll angle can be established. Since only the vehicle roll angle generated from lateral tire force is of interest as far as RSC is concerned, lateral acceleration is the solely input to this model, (i.e., bump or vertical force induced vehicle roll is not described),

$$\frac{d}{dt}\begin{bmatrix} \hat{\phi}_s \\ \dot{\hat{\phi}}_s \end{bmatrix} = \begin{bmatrix} 1 & 0 \\ -k_s & -c_s \end{bmatrix}\begin{bmatrix} \hat{\phi}_s \\ \dot{\hat{\phi}}_s \end{bmatrix} + \begin{bmatrix} 0 \\ Mh/I_x \end{bmatrix} a_y, \tag{20}$$

where $\hat{\phi}_s$ is the suspension roll angle estimate, k_s and c_s are spring stiffness and damping coefficient, respectively, I_x is the sprung mass roll moment of inertia, M is the mass of the sprung mass, h is the distance between the sprung mass center and roll center.

3.2.3 Arbitration and Summation: Since the lateral accelerometer generating the road bank angle described above is located on the vehicle sprung mass, it is conceivable that the road angle estimate may contain a suspension roll

angle. To be exact, suspension roll angle is contained in the estimated value obtained in 3.2.1 during steady state maneuver (when $DFC = 0$) but is not when the maneuver is very dynamic (when $DFC > 1$). Since the use of a dynamic factor in eliminating the lateral velocity derivative component has a side effect of eliminating the suspension roll angle, an arbitration scheme that utilizes the compliment of dynamic factor, or $\max(0, 1 - |DFC|)$, can provide the missing suspension roll angle as needed. This allows us to increase the fidelity of Euler roll angle estimation at higher frequencies without the concern of including suspension roll angle twice.

The summation and arbitration scheme is,

$$\hat{\phi} = \hat{\phi}_{dyn\_freq\_weighted} + \hat{\phi}_{sus\_freq\_weighted}, \tag{21}$$

where $\hat{\phi}_{sus\_freq\_weighted}$ is obtained as in Fig.3. Note that the

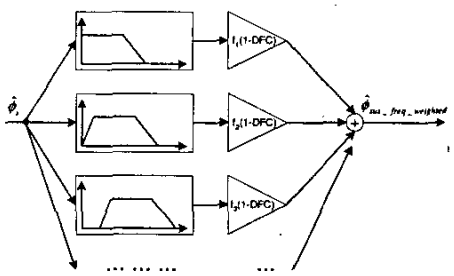

Figure 3: Frequency Weighted Suspension Roll Angle

arbitration schemes shown in Fig.2 and Fig.3, are designed to ensure the two processed components before the final summation, i.e., $\hat{\phi}_{dyn\_freq\_weighted}$ and $\hat{\phi}_{sus\_freq\_weighted}$, are mutually exclusive.

3.3 Roll Rate Measurement Compensation

The roll rate sensor is subject to both electrical and kinematic bias. For example, temperature change may cause output drift within sensor specification, and certain maneuvers/road conditions may induce a measurement bias. Therefore the raw sensor signal, denoted as ω_{x_raw}, should be properly compensated for all signal biases before it can be used to generate residual to avoid false detection.

3.3.1 Steady State Compensation for Electrical Bias: The raw roll rate signal ω_{x_raw} can be compensated by removing the sensor electrical bias ε

$$\omega_x = \omega_{x\_raw} - \varepsilon, \tag{22}$$

where ε is unknown and needs to be learned/updated. *With the virtue of vehicle roll rate signal equals to zero during straight driving*, ε can be adjusted in such a way that the following cost function $J_\varepsilon = |\omega_x|$ is minimized. To make J_ε small, it is reasonable to change ε in the direction of the negative gradient of J_ε [14], that is

$$\frac{d\varepsilon}{dt} = -\gamma_\varepsilon \frac{\partial J_\varepsilon}{\partial \varepsilon} = -\gamma_\varepsilon \frac{\partial \omega_x}{\partial \varepsilon} \mathrm{sgn}(\omega_x) = \gamma_\varepsilon \cdot \mathrm{sgn}(\omega_x), \tag{23}$$

where γ_ε is the adaptation rate. Note that the partial derivative $\frac{\partial \omega_x}{\partial \varepsilon}$ in (23) is evaluated under the assumption that ε is a constant, which is valid since sensor electrical bias changes much slower than other variables in the system.

3.3.2 Dynamic Compensation for Kinematic Bias: The roll rate signal generated from an on-board gyro sensor contains a kinematic bias, a quantity relating the inertial frame and the rotating frame. Since the roll rate of interest is the one relative to the inertia frame, a proper compensation has to be performed to remove this kinematics-induced bias, which is mostly the product of pitch angle θ and yaw rate ω_z. To be exact, the Euler roll rate (of the inertial frame) is [15]

$$\dot{\phi} = \omega_x + \sin\phi \cdot \tan\theta \cdot \omega_y + \cos\phi \cdot \tan\theta \cdot \omega_z, \tag{24}$$

where ω_y is the pitch rate of the rotating frame. Note ω_x is obtained from (22). To illustrate the significance of this bias removal, consider a vehicle going down a spiraled parking ramp of 6° grade with a yaw rate of, say, $10°/s$. The roll rate sensor will read as much as $1°/s$ even though the vehicle stays true parallel to the parking ramp at all time. Since this bias is kinematics-induced and not a fault of the roll rate sensor, they should be compensated to avoid being interpreted as a fault and a proper compensation should be performed before the sensed roll rate signal is fed into the designed observer.

To compensate the kinematics induced bias, we simplify equation (24) to estimate the Euler pitch angle,

$$\dot{\phi} \approx \omega_x + \vartheta \cdot \omega_z, \tag{25}$$

where a shorthand notation $\vartheta = \tan\theta$ is used. *With the virtue of vehicle Euler roll rate signal equals to zero during steady state turning*, ϑ can be adjusted in such a way that the following cost function $J_\vartheta = |\dot{\phi}|$ is minimized. Similar to (23), the adaptation law can be determined by a so-called *sign-sign algorithm* [14]

$$\frac{d\vartheta}{dt} = -\gamma_\vartheta \cdot \mathrm{sgn}\left(\frac{\partial \dot{\phi}}{\partial \vartheta}\right) \cdot \mathrm{sgn}(\dot{\phi}) = -\gamma_\vartheta \cdot \mathrm{sgn}(\dot{\phi} \cdot \omega_z), \tag{26}$$

in which the partial derivative $\frac{\partial \dot{\phi}}{\partial \vartheta}$ is evaluated under the assumption that ϑ is a constant, since the vehicle pitch angle changes slower than other variables in the system. γ_ϑ is the adaptation rate.

4 Simulation Results

To illustrate the robust fault detection scheme, simulations are performed based on the system (7) and the residual generator (11). Substituting (12) into (5) yields

$$r(s) = -WC(sI - A_c)^{-1}Kf_s + Wf_s = \frac{s}{s+\lambda_1} f_\phi - \frac{1}{s+\lambda_1} f_{d\phi/dt}. \tag{27}$$

The above equation suggests that the residual is most sensitive to low frequency roll rate measurement error, $f_{d\phi/dt}$, (*which is the critical failure mode*), and high frequency roll angle measurement error, f_ϕ, (*which seldom occurs in normal driving*). The transfer functions from f_ϕ and $f_{d\phi/dt}$ to residual are determined by λ_1 only, and are independent of the parameters in the A matrix of (10). When selecting the

observer poles, note that λ_1 should not be too large otherwise the DC gain of $\frac{1}{s+\lambda_1}$ will be reduced. On the flip side, if λ_1 is too small, it will be difficult to isolate $f_{d\phi/dt}$ from f_ϕ due to reduced bandwidth of both $\frac{s}{s+\lambda_1}$ and $\frac{1}{s+\lambda_1}$.

The design parameters and nominal values are chosen as:

$$\lambda_1 = 0.7,\ \lambda_2 = 1,\ k = 200,\ c = 100. \tag{28}$$

To illustrate the robustness of above design, the system (7) is subjected to large parametric uncertainties, i.e., $\Delta k = -300 + 50\sin(0.5t)$ and $\Delta c = -400 + 100\cos(0.2t)$. It is also subject to an unmeasured disturbance d, here in the shape of a square wave as in Fig.4. In addition to that, both sensors "fail" during the simulation. As shown in Fig.5, roll angle fault f_ϕ is a 1° shift occurs at $t = 2s$ and roll rate sensor fault $f_{d\phi/dt}$ is a $1^\circ/s$ shift occurs at $t = 10s$. The residual is shown in Fig.6, note how the residual is insensitive to model uncertainties (i.e, Δk, Δc, and d), and how it reacts differently to f_ϕ at $t = 2s$ and to $f_{d\phi/dt}$ at $t = 10s$, i.e., f_ϕ corresponds to a transient only while $f_{d\phi/dt}$ causes a steady state shift of the residual, which agrees with (27).

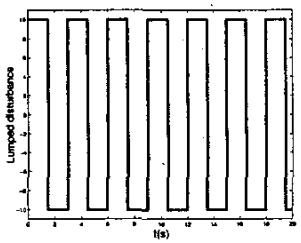

Figure 4: Disturbance

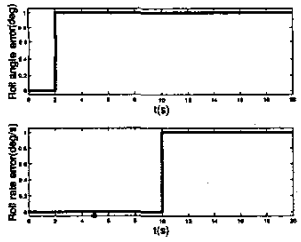

Figure 5: Sensor faults

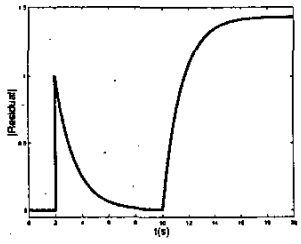

Figure 6: Residual

5 Experimental Verifications

While simulation results confirm the robust characteristics of the proposed robust observer, vehicle experimental verifications further substantiate real-world robustness and quantify the impact under road/vehicle/maneuvers disturbances. The proposed residual generator (11) is implemented with $y = [\hat{\phi}\ \ \dot{\phi}]^T$, with $\hat{\phi}$ and $\dot{\phi}$ defined in (21) and (25), using the developed roll angle estimation techniques and roll rate compensation techniques, respectively. The residual is then compared to a threshold. If the threshold is exceeded by the residual, the sensor is suspected to be at fault. The threshold is designed to be vehicle dynamics dependent. The idea is to keep the threshold tight for fast fault detection when the vehicle is operated in its normal conditions such as during regular maneuvers on normal road surfaces. When the vehicle is maneuvering through banked surfaces or is unstable, the threshold is increased for better robustness.

The experimental verifications of no false positive and/or no false negative were taken with a variety of maneuvers and road conditions with several vehicle test platforms. A few representative test results, especially the most challenging ones, are listed in Table 1. Fig.7 shows an aggressive slalom maneuver of a small SUV on a parabolic banked surface (whose bank angle varies from 0° to 20° depending on vehicle's lane positions). This test is especially challenging for robustness due to the difficulties in estimating correct vehicle roll angle during the maneuver which involves dynamically varying road bank angle (shown in Fig.8). The magnitude of the residual remains small, thanks to the proposed novel roll angle estimation technique and robust fault observer design. Fig.9 shows a high lateral acceleration ($a_y = 0.7g$) quasi-steady state cornering maneuver on dry asphalt. A $10^\circ/s$ roll rate fault was inserted during the maneuver and was promptly detected by the increased (and sustained) residual shown in Fig.10. Fig.11 shows a dynamic double lane change maneuver of a large SUV on gravel. Despite the dynamics involved and low surface μ, the residual exceeded the threshold at the insertion of a $10^\circ/s$ roll rate fault (Fig.12).

Table 1

Maneuvers	Fault	Detected?	False Alarm?
Mountain Drive	$10^\circ/s$	*Yes*	*N/A*
Double Lane Change	$10^\circ/s$	*Yes*	*N/A*
Constant Radius Turn	$10^\circ/s$	*Yes*	*N/A*
Lane Change on Gravel	$10^\circ/s$	*Yes*	*N/A*
ABS Braking	$10^\circ/s$	*Yes*	*N/A*
Spinning on Packed Snow	*N/A*	*N/A*	*No*
Fishhook	*N/A*	*N/A*	*No*
U Turn on 40% Grade	*N/A*	*N/A*	*No*
Mountain Drive	*N/A*	*N/A*	*No*
Bounce Sine Sweep	*N/A*	*N/A*	*No*

6 Conclusions

A model-based fault detection scheme has been presented to detect roll rate sensor failures in a vehicle roll stability control system. The method is based on a simple control-oriented vehicle roll model which is suitable for real-time diagnostic applications. A robust residual generator using eigenstructure assignment is constructed to make the detection insensitive to model uncertainties. The challenges of

implementing this strategy are discussed and addressed. Vehicle test results are presented to illustrate the effectiveness and the achievable performance of the proposed scheme.

References

[1] T. A. Brown and D. S. Rhode, "Roll over stability control for an automotive vehicle." United States Patent. Patent Number: 6324446, 2001.

[2] H. E. Tseng and T. Brown, "The development of vehicle stability control at Ford," *IEEE/ASME Transactions on Mechatronics*, vol. 4, no. 3, pp. 307–328, 1999.

[3] R. Isermann, "Process fault detection based on modeling and estimation methods: A survey," *Automatica*, vol. 20, no. 4, pp. 387–404, 1984.

[4] G. G. Leininger, "Model degradation effects on sensor failure detection," in *Proceedings of the 1981 Joint Automatic Control Conference*, vol. 2, (Charlottesville, VA), 1981.

[5] R. J. Patton and J. Chen, "Robust fault detection of jet engine sensor systems using eigenstructure assignment," *AIAA Journal of Guidance, Control, and Dynamics*, pp. 1666–1675, 1991.

[6] R. Patton, P. Frank, and R. Clark, *Fault Diagnosis in Dynamic Systems: Theory and Applications*. London: Prentice Hall International, 1989.

[7] M. Basseville and I. Nikiforov, *Detection of Abrupt Changes: Theory and Application*. Englewood Cliffs, N.J.: Prentice Hall, Inc., 1993.

[8] R. Eger, R. Majjad, and N. Nasr, "Rollover simulation based on a nonlinear model," *SAE No. 980208*, 1998.

[9] J. Bernard, J. Shannan, and M. Vanderploeg, "Vehicle rollover on smooth surfaces," *SAE No. 891991*, 1989.

[10] Y. Fukada, "Estimation of vehicle side-slip with combination method of model observer and direct integration," in *Proceedings of AVEC'98*, pp. 201–206, 1998.

[11] A. Nishio, K. Tozu, H. Yamaguchi, K. Asano, and Y. Amano, "Development of vehicle stability control system based on vehicle sideslip angle estimation," *SAE No. 2001-01-0137*, 2001.

[12] H. E. Tseng, "Dynamic estimation of road bank angle," in *Proceedings of AVEC 2000*, pp. 421–428, 2000.

[13] J. Y. Wong, *Theory of Ground Vehicles*. John Wiley & Sons, INC., 3rd ed., 2001.

[14] K. J. Astrom and B. Wittenmark, *Adaptive Control*. Addison-Wesley Publishing Company, Inc, 2nd ed., 1995.

[15] D. T. Greenwood, *Principles of Dynamics*. Prentice Hall, INC., 2nd ed., 1988.

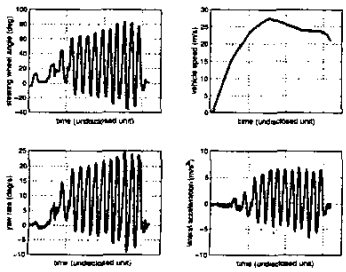

Figure 7: Vehicle States (Slalom on Banked Surface)

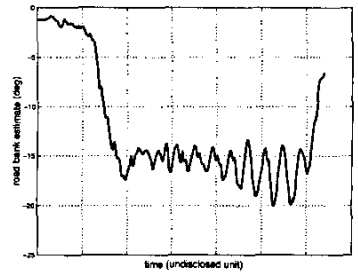

Figure 8: Estimated Road Bank Angle

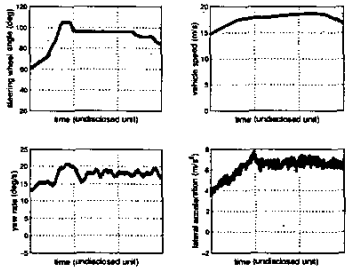

Figure 9: Vehicle States (0.7g constant radius turn)

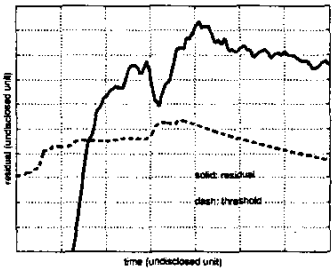

Figure 10: Residual and Threshold (0.7g constant radius turn)

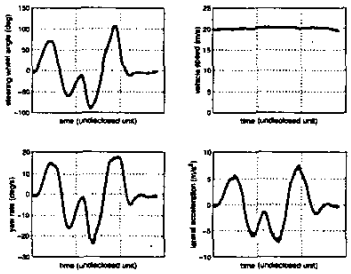

Figure 11: Vehicle States (Double Lane Change)

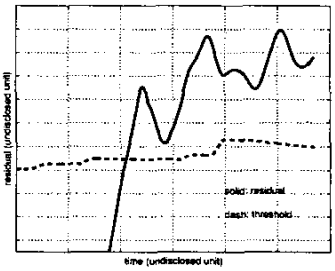

Figure 12: Residual and Threshold (Double Lane Change)